Analysis of supercritical methane in rocket engine cooling channels

Denies, Luka; Zandbergen, Barry; Natale, P.; Ricci, D.; Invigorito, M.

ANALYSIS OF SUPERCRITICAL METHANE IN ROCKET ENGINE COOLING CHANNELS

Luka Denies [(1)] , **Barry Zandbergen** [(1)], **Pasquale Natale** [(2)], **Daniele Ricci** [(2)], **and Marco Invigorito** [(2)]

[(1)]*Delft University of Technology, Kluyverweg 1, 2629 HS Delft, the Netherlands, Email: b.t.c.zandbergen@tudelft.nl*

[(2)]*Centro Italiano di Ricerche Aerospaziali, Via Maiorise, 81043 Capua (CE), Italy, Email: p.natale@cira.it*

ABSTRACT:

Methane is a promising propellant for liquid rocket engines. As a regenerative coolant, it would be close to its critical point, complicating cooling analysis. This study encompasses the development and validation of a new, open-source computational fluid dynamics (CFD) method for analysis of methane cooling channels. Validation with experimental data has been carried out, showing an accuracy within 20 K for wall temperature and 10% for pressure drop. It is shown that the turbulence model has only a limited impact on the simulation results and that the wall function approach generates valid results. Finally, a cooling analysis is performed to compare two thrust chamber materials. A traditional copper alloy is compared to aluminium as chamber material for a small moderate-pressure oxygen/methane engine. The analyses show that aluminium is a feasible chamber material only if a thermal barrier coating is applied. In addition, a significantly higher cooling channel pressure drop is incurred for an aluminium chamber than for a copper chamber due to the lower allowable temperature.

1. INTRODUCTION

An interesting propellant combination candidate for future space launch vehicles is oxygen/methane. Up to now, most liquid rocket engines that have flown burnt either a hypergolic propellant combination, oxygen/kerosene or oxygen/hydrogen. In the past years, several groups have initiated development programs to demonstrate methane-fuelled engines. In addition, both Blue Origin and SpaceX have announced they are developing large oxygen/methane first stage engines for orbital launch vehicles.

The critical point of methane occurs at a temperature of 190.56 K and a pressure of 4.599 MPa [1]. In rocket engines with low to moderate combustion chamber pressure, the methane cooling would be close to the critical pressure, also crossing the critical temperature. This means that the fluid property variations are important to take into account.

Pizzarelli developed an in-house finite-volume 3D CFD solver at "La Sapienza" University of Rome that is capable of analyzing the flow of methane in cooling channels [2]. The turbulence model used is the Spalart-Allmaras one-equation model. In a recent paper, the method was validated with experimental data [3].

The group of Hua Meng at Zhejiang University has published several papers on CFD analysis of methane coolant channels [4, 5, 6]. Wang et al. demonstrate a simple axisymmetric two-dimensional CFD method in [4]. They complement the Navier-Stokes equation with a shear stress transport (SST) $k - \omega$ turbulence model. Ruan et al. [5] and Wang et al. [6] from the same group report using the FLUENT program to perform CFD analysis on methane cooling channels. In both papers, the two-equation standard $k - \epsilon$ turbulence model is implemented with Wolfstein wall modelling [5, 6]. Experimental validation was only carried out with supercritical carbon dioxide and n-heptane by these researchers.

Negishi et al. report the use of CRUNCH CFD software for analysis of methane coolant channels [7]. This is an unstructured, three-dimensional flow solver using a cell-vertex finite volume discretization. The high-Reynolds $k - \epsilon$ turbulence model was used by Negishi et al, together with the Wolfstein near-wall treatment [7]. The results obtained from this simulation were validated with experimental results from two subscale methane/oxygen engine firings [7].

A wide array of CFD methods has been applied to analyse methane channels. It is noticeable that no investigation has been reported to date on the influence of the turbulence model. Secondly, all methods are closed-source. In this paper, the effect of the turbulence model will be examined by means of an open-source CFD method that is freely available.

Traditionally, the launcher industry uses copper alloys as wall material in regeneratively cooled combustion chambers. They offer a high allowable temperature and high thermal conductivity, but are also heavy and expensive. Recently, XCOR and Masten Space Sys-

tems have demonstrated aluminium combustion chambers. Aluminium alloys have weight and cost advantages, but have lower allowable temperature and thermal conductivity. Tab. 1 shows a rough comparison of the relevant properties of copper and aluminium.

Table 1. Typical properties of copper and aluminium alloys for thrust chamber construction

Property	Copper	Aluminium
T_{allow} [K]	800 K	500 K
k [W/m $\cdot$ K]	300-400	100-200
ρ [kg/m^3]	9100	2800
Cost	High	Low

In the current paper, the feasibility of using aluminium for the chamber wall of a regeneratively cooled oxygen/methane rocket engine is investigated.

2. NUMERICAL METHOD

Computational fluid dynamics was used to solve the flowfield inside rocket engine channels. This CFD simulation was coupled to a heat conduction simulation inside the solid wall material, creating a conjugate heat transfer (CHT) analysis. Section 2.1 describes in general the CFD setup that was used, while section 2.2 goes into detail how the properties of supercritical methane were obtained.

2.1. CFD setup

The open-source CFD package OpenFOAM was used for simulations. Because of the density variations in supercritical flows, a compressible solver was needed, solving the conservation equations Eq. 1, Eq. 2 and Eq. 3. The solver is pressure-based (using pressure-velocity-density coupling) and calculates a steady-state solution. Van Leer limiting was used for the validation cases, but for the rocket engine cooling channel simulations it was necessary to use upwind discretisation schemes to obtain stable solutions.

$$\nabla \cdot (\rho \mathbf{U}) = 0 \tag{1}$$

$$\nabla \cdot (\rho \mathbf{U}\mathbf{U}) = -\nabla p + \nabla \cdot \tau \tag{2}$$

$$\nabla \cdot (\rho h\mathbf{U}) + \nabla \cdot \left(\rho \frac{|\mathbf{U}|^2}{2} \mathbf{U} \right) = \nabla \cdot \tau \cdot \mathbf{U} + \nabla \cdot \kappa_{eff} \nabla T \tag{3}$$

In these equations, ρ refers to the fluid density, $\mathbf{U}$ to the fluid velocity vector, p to the pressure and T to the temperature. τ is the shear stress tensor, h is the enthalpy and κ_{eff} is the effective thermal conductivity (which includes a contribution due to turbulence).

Because of the high Reynolds number, the flow inside the channels is turbulent. Various researchers have applied different Reynolds-averaged Navier-Stokes (RANS) turbulence models to this problem. One of the aims of this research was to compare the models. Compressible formulations for Spalart-Allmaras [8], standard k-ϵ [9] and shear stress transport (SST) k-ω [10, 11] models, available in OpenFOAM, were used. To model the roughness of the channel wall and its influence on turbulence, two general approaches have been used. The first is the boundary layer integration approach, in which the boundary layer is fully integrated. This requires a high number of cells near the wall, with the first cell at $y^+ \approx 1$, y^+ being the dimensionless wall distance. For the Spalart-Allmaras model, the Boeing extension reported by Aupoix and Spalart was employed as a roughness correction [12]. For the k-ω SST model, the Nikuradse correction reported by Aupoix was used [13].

An alternative approach to correct for roughness is the wall function approach. With this method, the boundary layer is not fully integrated and the first cell is at $y^+ > 30$. Instead, the turbulence parameters of the first cell are modified to account for roughness, decreasing computation time. The standard wall functions available in OpenFOAM were used here.

To model conduction of heat through the wall, a form of the Fourier heat equation (Eq. 4) is used. Here c_p is the isobaric specific heat of the fluid.

$$0 = \nabla \cdot \left(\frac{\kappa}{c_p} \nabla c_p T \right) \tag{4}$$

2.2. Methane properties

To solve the governing equations, four fluid properties must be known: density ρ, enthalpy h, viscosity μ and thermal conductivity κ. All four must be known as a function of pressure and temperature, closing the system of equations.

The GERG-2004 equation of state was used to calculate density and enthalpy. Kunz et al. estimate that GERG-2004 offers an accuracy of 0.1% for methane density at pressures below 300 bar and temperatures between 100 K and 600 K [1]. Experimental data are represented to within 0.02-0.03%, but the accuracy of the model is limited by the accuracy of experimental data. The accuracy of enthalpy is approximately 1%, likewise limited by the accuracy of experimental data [1].

The used viscosity model is the friction theory model proposed by Quiñones-Cisneros and Deiters. For methane, it is valid in the region of 100-500 K with an average deviation of 0.83% and maximum deviation of 6.02% with respect to experimental data [14]. The thermal conductivity is based on three components: the di-

2

lute gas, excess and critical thermal conductivity. The former two terms are calculated using relations given by Sanokidou et al. [15]. The critical enhancement of thermal conductivity is calculated using equations from Olchowy and Sengers [16].

Fig. 1 shows a comparison between fluid property values calculated from the equations described above and the well-known NIST dataset [17]. The correct implementation of the relevant equations is verified in this way. NIST does however use older, less accurate equations, resulting in slight differences in Fig. 1, most notably in the thermal conductivity.
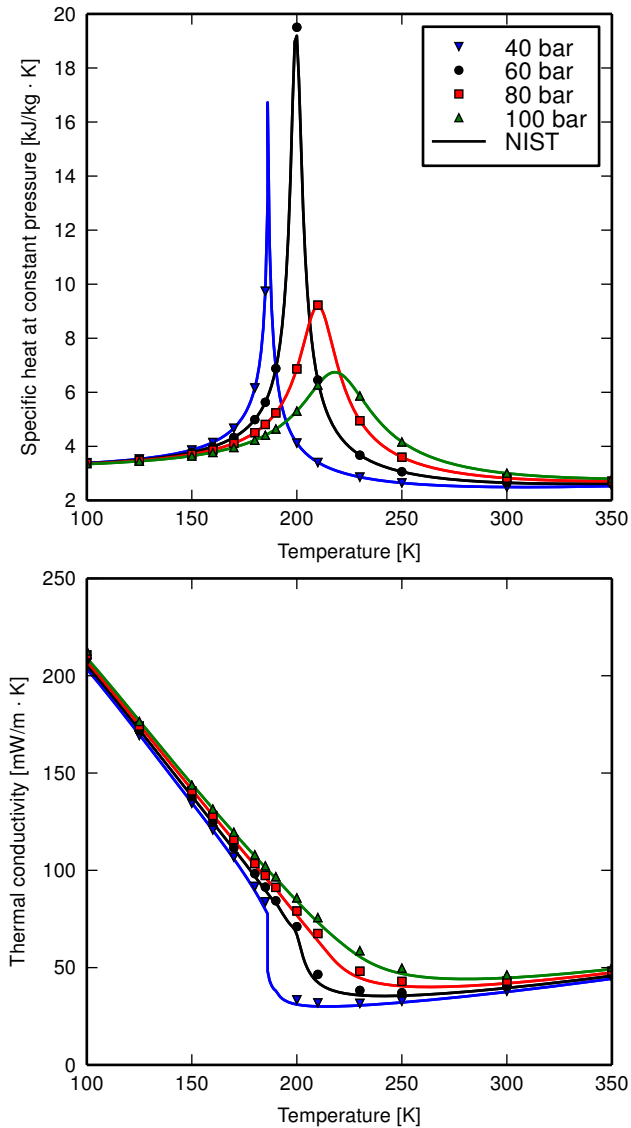

Figure 1. Comparison between fluid property models programmed in Python (markers) and NIST reference data [17] (curves)

The equations discussed in the previous paragraphs are complex and computationally demanding. Because the fluid properties must be calculated for each volume in the domain, the computation time increases dramatically when using these equations. To avoid this problem, the accurate but complex equations were used to create interpolation tables for ρ, h, μ and κ as a function of pressure and temperature. A bilinear interpolation is performed at runtime for each volume. This approach reduces the computation time while retaining the accuracy of the fluid property relations.

A non-structured set of (p, T) points is used to cluster data points around the critical point, where property variations are largest. The $\Delta\rho$ between data points is approximately 0.25 kg/m^3. This results in a maximum error of 0.015% between the density calculated from GERG-2004 and the interpolated value. Similar accuracy is obtained after interpolation other fluid properties, far better than the experimental accuracy of the equations themselves.

2.3. Hot gas side heat transfer

The hot gas side heat transfer in the thrust chamber was represented by semi-empirical equations: Bartz equation to represent convective heat transfer [18] and two relations by Kirchberger for radiative heat transfer by water (Eq. 5) and carbon dioxide (Eq. 6) [19]. In these relations, q_R refers to the radiative heat flux, R is the radius of the nozzle and the subscripts H_2O and CO_2 refer to water and carbon dioxide respectively.

$$q_{R,H_2O} = 5.74 \cdot \left(\frac{p_{H_2O}}{10^5} \cdot R \right)^{0.3} \left(\frac{T}{100} \right)^{3.5} \quad (5)$$

$$q_{R,CO_2} = 4 \cdot \left(\frac{p_{CO_2}}{10^5} \cdot R \right)^{0.3} \left(\frac{T}{100} \right)^{3.5} \quad (6)$$

3. VALIDATION

Experimental validation of the method was carried out using data from the MTP test campaign performed by CIRA. More detail on this test campaign is given in [20].

3.1. Experiment setup

The concept of the MTP Breadboard is based on the electrical heating of a conductive material (a copper alloy), where a narrow rectangular channel is realized. Heat fluxes result to be similar to those experienced by methane in the regenerative cooling jacket of a rocket and also the channel is featured by dimensions, typical of most LREs. The test article has a rectangular basement where 10 slots for the electrical cartridges (12 kW of maximum power) were realized, and has a parabolic

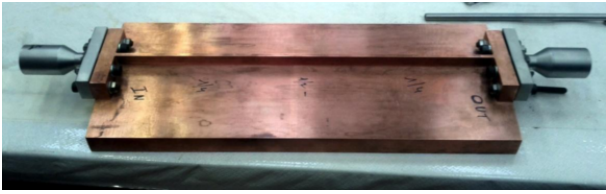profile on the top in order to drive the heat towards the channel.

Figure 2. MTP test specimen with hydraulic interfaces. Methane at supercritical pressure is pumped through the single channel and heated from the bottom.

Fig. 2 shows a photograph of the test specimen. The total length (including flanges) and width is equal to 316 mm and 125 mm, respectively, while the rectangular channel has an aspect ratio equal to 3. The effective length of the straight section is 292 mm. At the inlet and outlet sections two mechanical interfaces, threaded and sealed are provided: they are characterized by a length of 10 mm each and present external connections with holes compatible with common hydraulic interfaces. Pressure and temperature sensors are placed in the middle of the interfaces.The test article has been designed to be tested in this operative envelope.

Tests were successfully conducted at the Maurice J. Zucrow Laboratories, Purdue University. The channel, located at the top of the article (at the end of the parabolic lateral wall) was fed by methane at pressure and cryogenic temperature values, ranging from 8.0 to 15.0 MPa and 120 K to 140 K. The fluid was heated in order to obtain the transition through the critical conditions and beyond the pseudo-critical state.

The breadboard is equipped with twenty-four thermocouples: twelve in the basement and twelve in the close-out along the axial direction. The extremities are oriented towards the bottom and upper surface of the channel and placed at different depth (4, 10 and 16 mm). The mass flow was measured by means of a cavitating venturi. During the tests, the article was thermally insulated by a 1-cm-thick ceramic blanket to avoid losses of heat power throughout external walls.

3.2. Comparison with experimental data

The straight channel was simulated in OpenFOAM using the numerical method described earlier. In order to save setup and computation time, the inlet and outlet manifold geometry was not included. At CIRA, however, an analysis using Fluent that did include these manifolds had already been performed. This analysis was used to correlate the experimental pressure measurements to the OpenFOAM simulations.

The symmetry of the problem was exploited by simu-

lating only half of the channel in each case. Two grids were used: one for cases with boundary layer integration and one for case with wall functions. A fluid mesh of $350 \times 10 \times 30$ cells in length $\times$ half-base $\times$ height was chosen for the wall function approach. The first cell from the wall is at a distance of approximately $5 \cdot 10^{-5}$ m for all walls.

For the boundary layer integration approach, a fluid mesh of $200 \times 40 \times 100$ cells was finally designed. This mesh has a first cell at approximately $5 \cdot 10^{-7}$ m with a growth factor of 1.12 in both y and z directions.
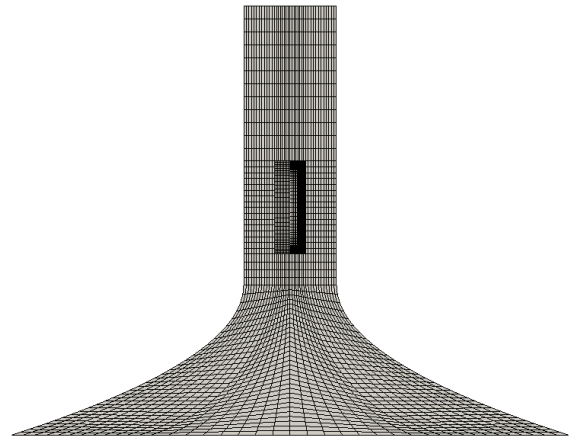

Figure 3. Cross-section of mesh for wall function (left) and boundary layer integration (right) approaches. The outer regions belong to the solid domain, the inner core is the fluid domain.

The solid domain is very similar for both meshes. The distribution of cells in a cross-section is exactly the same, with 1152 cells each. The number of cells in x direction equal for the fluid and solid domain. The curved edge of the domain was obtained from CIRA and conforms to shape of the test article that was used in the experiments. It is cut off at a distance of approximately 6 mm below the channel, because this was the limit of the shape obtained from CIRA. Fig. 3 shows a cross-section of the resulting meshes.

A cold flow test was rebuilt first to find the wall roughness. A value of 14.5 μm resulted in the correct pressure drop, so this value was adopted for the simulations of hot experimental runs.

Fig. 4 shows the comparison between the experimental pressure at inlet and outlet and the numerically calculated pressure evolution along the channel. An outlet pressure of 102.4 bar was prescribed at the end of the straight channel. Except for the k-ω model with boundary layer integration, all models agree fairly well with the Fluent prediction, which in turn is close to the experimental pressures.
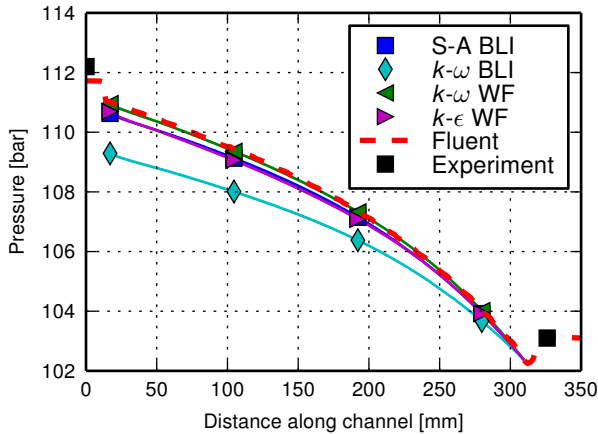
Figure 4. Pressure drop comparison for TC24. Note that the Fluent analysis performed by CIRA includes the hydraulic interfaces, where the pressure is measured. The OpenFOAM analyses do not include the interfaces. Experimental results and FLUENT analysis are courtesy of CIRA ScpA.

Fig. 5 shows the comparison of the wall temperatures measured by the thermocouples embedded at 4 mm depth with simulated wall temperatures. It is assumed that, due to thermocouple sensing and positioning inaccuracy, the temperature measurement is accurate to within 10 K. All models predict the wall temperature to within 20 K of the measured value for the three locations.
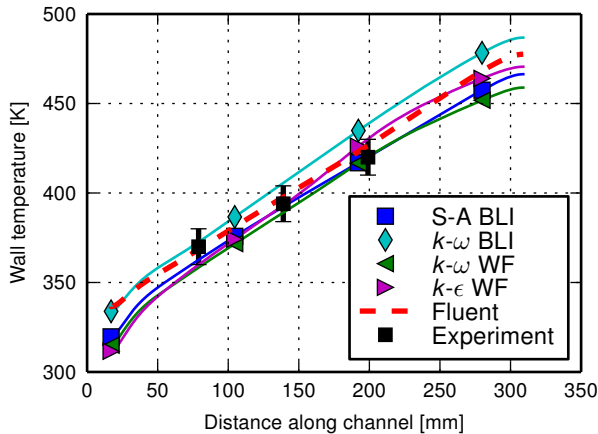

Figure 5. Comparison of temperature of embedded thermocouples at 4 mm with numerical results for TC24. Experimental results and FLUENT analysis are courtesy of CIRA ScpA.

The results of the experimental validation are satisfying on several levels. Three of the tested modelling approaches predict the pressure drop in the channel within 10% of the experimental value. They simultaneously predict the wall temperature within 15 K at the three measured locations. Furthermore, two of these successful models use wall functions instead of boundary layer integration which significantly reduces the required computation time.

The Spalart-Allmaras model gives the best agreement with thermocouple data, while the k-ω model gives the best comparison with pressure data when corrected for pressure drop at the interfaces. The calculation time for the boundary layer integration methods is almost 20 times as high as for the wall function methods. Taking these considerations into account, the k-ω SST model with wall function approach was selected for further analysis.

The data from another test case (TC43) resulted in a similar agreement between experimental data and numerical modelling. However, caution should be exercised when generalising these results. One reason for caution is that the pressures were substantially higher than the critical pressure. It is likely that the wall function approaches will not be as accurate when phenomena like heat transfer deterioration are present. Another reason for caution is that the total temperature range in the experiment was limited, the maximum temperature was around 400 K. In case there is a wider temperature range, the accuracy may be affected. Lastly, the experiment considered a constant rectangular cross-section. True rocket engine channels will have varying dimensions and curvature, which complicates the flow pattern. Because of these reasons, a temperature margin of 50 K was employed when using the method.

4. RESULTS

The successfully validated CFD method was used to investigate regenerative cooling of an oxygen/methane thrust chamber. The subject of study was a generic chamber with a design thrust of 10 kN – a potential engine design that is under scrutiny by the student association Delft Aerospace Rocket Engineering [21]. The aim of the study was to explore the options for construction of the thrust chamber and cooling channels in terms of material choice and geometry. One goal was to determine the feasibility of using an aluminium alloy instead of copper for the chamber wall.

Both the radial symmetry of the engine and the symmetry of the cooling channels themselves are used to reduce the domain size: only half of a single channel is simulated. Of this channel, both the methane coolant and the chamber wall (inner wall, rib and outer wall) are simulated. The black line in Fig. 6 shows the nozzle contour of the engine under investigation.
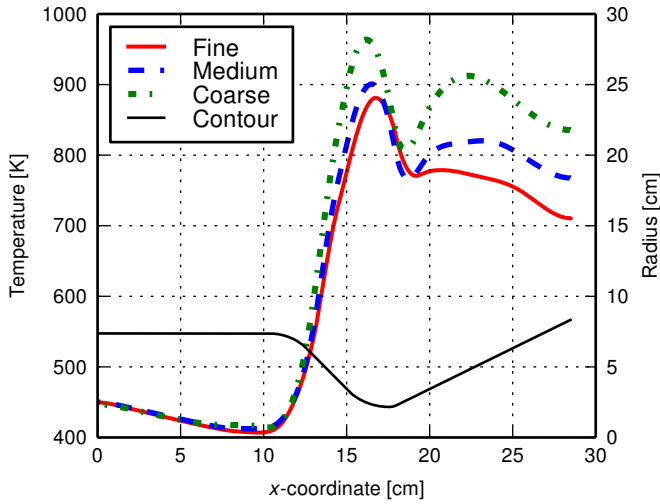
Figure 6. Grid convergence of wall temperatures obtained for a single case

The required number of cells in the directions towards the wall was determined by the y^+ value required by wall function approaches. 24×16 cells were used for the half-base × height of the channel. For the number of cells in streamwise direction, a grid convergence study was performed. Fig. 6 shows the wall temperature for the same case with 125, 250 and 500 cells in streamwise direction. Clearly, the temperature profiles are converging. The number of 500 cells was adopted for the remaining simulations.
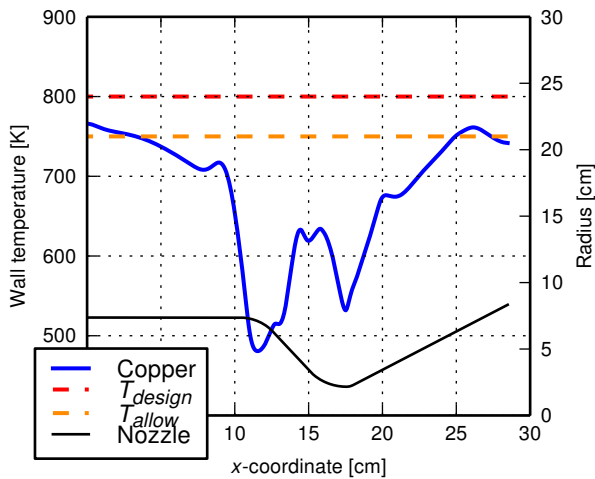

Figure 7. Wall temperatures obtained for copper chamber. The peaks and valleys are due to the specific channel geometry.

Taking into account the design margin of 50 K, the aim was to design a cooling channel geometry that kept the wall temperature below the design temperature at all locations inside the nozzle. The channel height profile was changed manually after each simulation. Fig. 7 shows the result for a copper chamber, where the wall temperature is below 750 K at almost all locations. The pressure drop for this design is 14 bar.

Fig. 7 shows that there are strong temperature variations along the wall for this particular channel design. The channel height is shown in Fig. 8. The temperature minima around x =11 cm and 17 cm are due to a local narrowing of the channel.
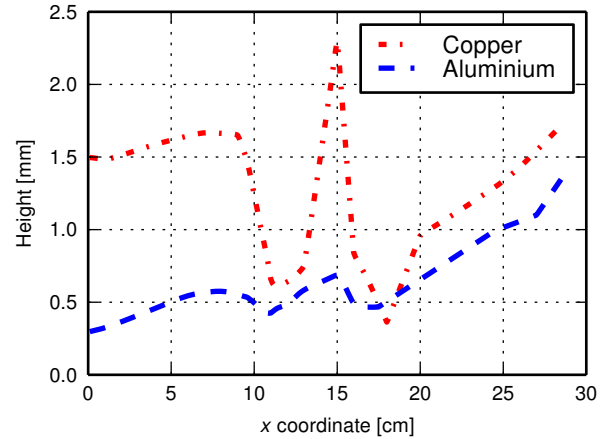

Figure 8. Channel height comparison between copper and aluminium chamber. The channels of the aluminium chamber need to be more narrow because of the lower allowed temperature.

It was found that, for an aluminium chamber which is cooled only regeneratively, insulation of the chamber wall is necessary. This can be obtained either by applying a thermal barrier coating or by anodizing the surface to create a layer of aluminium oxide. For the remainder of the study, it was assumed that a layer of 50 μm thickness and 1 W/m · K thermal conductivity was present on the aluminium chambers. Such a layer could feasibly be created using either hard anodizing or a zirconium oxide coating [22, 23].

Even with a thermal barrier coating present, the aluminium chamber required substantially higher coolant velocities. These can be obtained by decreasing the channel dimensions, in this case the height of the channels. Fig. 8 shows a comparison of the height for an aluminium chamber and a copper chamber. The resulting wall temperature is displayed in Fig. 9. Tab. 2 shows a comparison of the design of the copper and aluminium chambers.
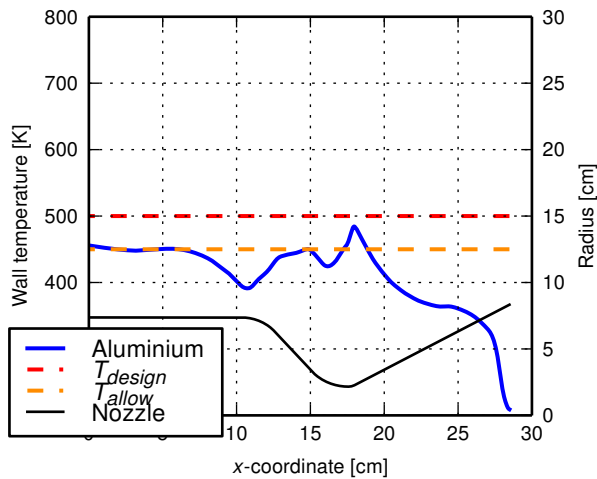
Figure 9. Wall temperatures obtained for aluminium chamber. The peaks and valleys are due to the specific channel geometry.

Table 2. Design of copper and aluminium chambers

Property	Copper	Aluminium
Design temperature [K]	750	450
Number of channels [-]	64	80
Pressure drop [bar]	14	44
Mass [kg]	1.3	0.37
Thermal barrier coating	No	Yes

The analysis shows that an aluminium chamber is in principle feasible, if the chamber is coated. However, the increased pressure drop has consequences on the system level, i.e. the tank pressure must increase to cope with the higher pressure drop. It was therefore examined what the impact on tank mass would be for a small pressure-fed system. For a propellant mass of 100 kg of methane, it was analysed how much heavier a spherical tank would have to be to accommodate the higher required pressure.

Assuming the tank pressure equals 50 bar plus the pressure drop over the channels and the tank is made out of a generic aluminium alloy in both cases, it turns out that the tank of the aluminium engine would need to be 8 kg heavier. This is a much more substantial effect than the small mass decrease on engine level! For a pump-fed system, the effect will not be as pronounced. Nonetheless, the point remains: to regeneratively cool an aluminium thrust chamber, a high increase in pressure drop is required, which has severe effects on the system level.

5. CONCLUSIONS AND RECOMMENDATIONS

A new, open-source method was developed to analyse methane cooling at supercritical pressure – available online at [24]. The method was validated by comparison with experimental data from the MTP test campaign conducted by CIRA. Wall temperature accuracy was found to be 20 K, while the pressure drop was accurate to within 10%.

The method was then used to perform a cooling analysis for a copper and aluminium thrust chamber, intended for a 10 kN oxygen/methane rocket engine. The analysis showed that aluminium chambers are in principle feasible, if a thermal barrier coating is applied. However, the pressure drop increases dramatically. For a pressure-fed propulsion system, the tank mass penalty associated with the higher pressure drop is much more severe than the thrust chamber mass saving as a result of an aluminium chamber.

REFERENCES

1. Kunz, O., Klimeck, R., Wagner, W., and Jaeschke, M. (2007). The GERG-2004 Wide-Range Equation of State for Natural Gases and Other Mixtures. Technical Report GERG TM15 2007, Groupe Européen de Recherches Gazières, Düsseldorf, 2007.

2. Pizzarelli, M. (2007). *Modeling of Cooling Channel Flow in Liquid-Propellant Rocket Engines*. PhD thesis, Universita degli Studi di Roma "La Sapienza", 2007.

3. Pizzarelli, M., Nasuti, F., Votta, R., and Battista, F. (2015). Assessment of a Conjugate Heat Transfer Model for Rocket Engine Cooling Channels Fed with Supercritical Methane. In *51st AIAA/SAE/ASEE Joint Propulsion Conference*, AIAA 2015-3852.

4. Wang, Y.-Z., Hua, Y.-X., and Meng, H. (2010). Numerical Studies of Supercritical Turbulent Convective Heat Transfer of Cryogenic-Propellant Methane. *Journal of Thermophysics and Heat Transfer*, **24**(3), 490–500.

5. Ruan, B. and Meng, H. (2012). Supercritical Heat Transfer of Cryogenic-Propellant Methane in Rectangular Engine Cooling Channels. *Journal of Thermophysics and Heat Transfer*, **26**(2), 313–321.

6. Wang, L., Chen, Z., and Meng, H. (2013). Numerical study of conjugate heat transfer of cryogenic methane in rectangular engine cooling channels at supercritical pressures. *Applied Thermal Engineering*, **54**(1), 237–246.

7. Negishi, H., Daimon, Y., Kawashima, H., and Yamanishi, N. (2012). Flowfield and Heat Transfer Characteristics of Cooling Channel Flows in a Methane-Cooled Thrust Chamber. In *48th AIAA/ASME/SAE/ASEE Joint Propulsion Conference & Exhibit*, AIAA 2012-4122, Atlanta.

8. Spalart, P. R. and Allmaras, S. R. (1992). A One-Equation Turbulence Model for Aerodynamic Flows. In *30th Aerospace Sciences Meeting & Exhibit*, AIAA-92-0439, Reno.

9. El Tahry, S. H. (1983). k-ϵ equation for compressible reciprocating engine flows. *Journal of Energy*, **7**(4), 345–353.

10. Menter, F. R. (1993). Zonal Two Equation $k-\omega$ Turbulence Models for Aerodynamic Flow. In *24th Fluid Dynamics Conference*, AIAA 93-2906, Orlando.

11. Menter, F. R., Kuntz, M., and Langtry, R. (2003). Ten Years of Industrial Experience with the SST Turbulence Model. *Turbulence Heat and Mass Transfer 4*, pages 625–632.

12. Aupoix, B. and Spalart, P. R. (2003). Extensions of the Spalart - Allmaras turbulence model to account for wall roughness. *International Journal of Heat and Fluid Flow*, **24**(4), 454–462.

13. Aupoix, B. (2014). Roughness Corrections for the $k-\omega$ Shear Stress Transport Model: Status and Proposals. *Journal of Fluids Engineering*, **137**(2), 021202.

14. Quiñones-Cisneros, S. E. and Deiters, U. K. (2006). Generalization of the Friction Theory for Viscosity Modeling. *Journal of Physical Chemistry B*, **110**(25), 12820–12834.

15. Sakonidou, E. P., van den Berg, H. R., ten Seldam, C. A., and Sengers, J. V. (1996). The thermal conductivity of methane in the critical region. *The Journal of Chemical Physics*, **105**(23), 10535–10555.

16. Olchowy, G. A. and Sengers, J. V. (1989). A Simplified Representation for the Thermal Conductivity of Fluids in the Critical Region. *International Journal of Thermophysics*, **10**(2), 417–426.

17. NIST Chemistry WebBook. Available online at `http://webbook.nist.gov/chemistry/`. Accessed April 11, 2015.

18. D.R.Bartz (1957). A simple equation for rapid estimation of rocket nozzle convective heat transfer coefficient. *Jet Propulsion*, **27**(1), 49–51.

19. Kirchberger, C. U. (2014). *Investigation on Heat Transfer in Small Hydrocarbon Rocket Combustion Chambers*. PhD thesis, Technische Universität München, 2014.

20. Votta, R., Battista, F., Gianvito, A., Smoraldi, A., Salvatore, V., Pizzarelli, M., Leccese, G., Nasuti, F., Shark, S., Feddema, R., and Meyer, S. (2014). Experimental Investigation of Methane in Transcritical Conditions. In *50th AIAA/ASME/SAE/ASEE Joint Propulsion Conference*, AIAA 2014-4005, Cleveland.

21. Wink, J., Hermsen, R., Huijsman, R., Akkermans, C., Denies, L., Barreiro, F., Schutte, A., Cervone, A., and Zandbergen, B. (2016). Cryogenic Rocket Engine Development at Delft Aerospace Rocket Engineering. In *Space Propulsion Conference 2016*, SP2016-3124644, Rome. To be published.

22. Lee, J., Kim, Y., Jung, U., and Chung, W. (2013). Thermal conductivity of anodized aluminum oxide layer: The effect of electrolyte and temperature. *Materials Chemistry and Physics*, **141**(2-3), 680–685.

23. Nesbitt, J. A. (1990). Thermal Response of Various Thermal Barrier Coatings in a High Heat Flux Rocket Engine. *Surface and Coatings Technology*, **43-44**(1), 458–469.

24. Denies, L. (2015). OpenFOAM module for tabulated fluid properties, July 2015. Available online at `https://github.com/ldenies/tabulatedProperties`. Accessed November 26, 2015.